Volumetric strain measurement of polymeric materials subjected to uniaxial tension

Marius Andersen[1,2], Odd Sture Hopperstad[1] and Arild Holm Clausen[1]

[1] Centre for Advanced Structural Analysis (SFI-CASA), Department of Structural Engineering, Norwegian University of Science and Technology (NTNU), NO-7491 Trondheim, Norway

[2] SINTEF Industry, Materials and Nanotechnology, NO-7465 Trondheim, Norway

Abstract

A novel method for measuring and calculating volumetric strain in circular-cylindrical uniaxial tension samples made from polymeric materials is proposed. It is shown that special considerations must be taken when calculating volumetric strain when a sample is in a post-necking state. Solely based on surface data, the key feature of the proposed correction is that it allows for an inhomogeneous distribution of longitudinal strain through the diameter of the sample, where a more traditional approach would be to assume a homogeneous distribution. These two approaches are evaluated by applying them to data from a close-to-incompressible steel sample. Whereas the proposed method indicates only a small positive increase in volume, the assumption of a homogeneous distribution results in substantial negative volumetric strains. Applying the two methods to tension samples made from HDPE and PVC, where plastic dilatation is nonlinear, again shows an initial negative volumetric strain for HDPE with the assumption of a homogeneous longitudinal strain. The proposed method predicts close-to-zero early stage volumetric strain for the same test. The differences are more subtle for samples of PVC. Micrographs obtained with scanning electron microscope show that the dilatation of PVC is related to voiding of the material around filler particles, while the underlying mechanism for HDPE is less clear. The results indicate that earlier reports of negative volumetric strain in polymers subjected to uniaxial tension might be artefacts of the implicit assumption made when calculating the volumetric strain.

1. Introduction

The last decades have seen an increase in the use of polymers in load carrying and shock absorbing components. As a consequence comes the requirement of predicting the material behavior of components subjected to various loading conditions in numerical simulations. Such material models should be able to describe the material response at large deformations and at different strain rates. Material failure is also highly relevant in cases where the polymer is used in protective or shock absorbing components.

Unlike most other materials, a particular feature of polymers is that they may exhibit substantial plastic volume increase when subjected to a tension-dominated hydrostatic stress state. This has been reported for both neat polymers [1-3] and polymers that have added particles [1, 4-8]. Several different mechanisms depending on the material and the loading conditions may contribute to the volume increase. Thus, the origin of plastic dilatation can be attributed to phenomena such as local cavitation [9], particle-matrix debonding [10],[11], and crazing [12-14]. The subsequent void growth leads to a macroscopic increase of volume. By measuring the volume increase during loading, these phenomena can be quantified and modeled, allowing for predictive models for the failure of polymers. Such models can then be implemented into finite element codes to better evaluate and predict the response of polymer components subjected to significant plastic deformations, relevant for applications such as protective structures and crash analyses.

Careful studies of the dilatation process and the underlying mechanisms require tests where the hydrostatic stress state is varied. This is usually accomplished by use of notched samples having different notch radii, see for instance Boisot et al. [3]. On the other hand, uniaxial tension tests on smooth specimens are the primary way of acquiring data on the behavior of polymers in an industrial environment. The information from uniaxial tension tests is used to identify the parameters in a material model. It is of utmost importance for the confidence of the numerical simulations of the design problem at hand that accurate stress and strain data is gathered from the test, and such data has to take possible volume changes into account. Application of pressure-dependent yield functions or plastic potentials in a material model implies that the plastic dilatation has to be accurately measured experimentally for determination of the relevant material parameters. As most ductile polymers experience necking at a comparatively early stage of a uniaxial tension test, local measurements are necessary to obtain precise strain data.

Image based techniques seem to be the most widespread tool for measuring local deformation in polymer samples. This was pioneered by G'sell et al. [15]. They applied some discrete markers to a tension test sample with a small geometrical imperfection, and used an *in-situ* technique to characterize the post-necking behavior of the polymer at hand. A more general method is to monitor the test sample with a digital camera, and analyze pictures of the sample during the deformation process with digital image correlation (DIC) [16]. This method gives a complete two-dimensional strain field at the surface, but is computationally more expensive. DIC has successfully been employed in a large number of studies of polymers [8, 17-21], and it has also become more common to use in industrial projects. Another application of the digital pictures is edge tracing. This method gives direct information about the change of specimen width or diameter, and hence the transverse strains [22, 23].

To determine volumetric strain, measurements of the in-plane and out-of-plane deformation fields are required. In general, this calls for two cameras and application of stereo-DIC in the subsequent data analysis. On the other hand, Johnsen et al. [18] monitored a test on an XLPE material with two perpendicular cameras, and compared the results obtained with 2D and 3D DIC. They found that it was almost no difference between the two methods. Thus, an

instrumentation protocol involving one camera is sufficient provided that the deformation in the two transverse directions of the specimen is the same.

The classic way to calculate the volumetric strain is to add the three normal strain components measured in the longitudinal and two transverse directions, see Section 2.1. If the normal strain components are determined from surface measurements, this approach may give a significant and rather surprising decrease of volume when stretching a sample [24-29]. A more fundamental issue is addressed by Laiarinandrasana et al. [30]. They applied X-ray tomography on a PA6 material, and showed that the radial distribution of voids and hence the volumetric strain is complex. Thus, the accuracy of volumetric strains determined from surface measurements can be questioned. Nevertheless, improved methods for calculation of the strain field have been proposed in the literature. Rossi et al. [21] have made a recent contribution, where they represent the internal displacement field with Bézier curves. A more advanced way to determine the change of volume is to employ computer tomography (CT). This technique allows for quantification of voided volume within the material. A drawback, however, is the comparatively long acquisition time. Nevertheless, some *in situ* studies incorporating CT during a tension test are available. Brusselle-Dupend et al. [31] applied a synchrotron to obtain full-field measurements of the voiding process during a tension test on PVF2. Later, Poulet et al. [9] considered a PA11 material.

Yet, the most common instrumentation protocol for material tests of polymeric materials is still digital cameras and a subsequent analysis of the pictures with DIC, resulting in data on the strain field at the surface. During material characterization in an industrial design process, it is very useful to have a closed-form equation for the volumetric strain, even though it is approximative. It will be demonstrated in this article that the classic formula for calculation of volumetric strain must be modified when the deformation of the tension specimen is non-homogeneous, such as during necking. Based on geometrical considerations, an improved closed-form equation is proposed in Section 2.2, and it is validated with test data on an incompressible material in Section 2.3. The proposed method for calculation of the volumetric strain applies DIC in combination with edge tracing. The DIC algorithm is based on higher order interpolation elements. These elements are advantageous compared with linear elements when measuring the longitudinal strain in the neck. The edge tracing technique is used to characterize the average local transverse strain and the curvature of the necked sample [22]. Section 3 pays attention to the volumetric response of high-density polyethylene (HDPE) and polyvinylchloride (PVC) when subjected to uniaxial tension. Finally, some concluding remarks are provided in Section 4.

2. Calculation of volumetric strain

2.1. Classic method

In the case of a tension sample with a circular cross section, the volumetric strain can easily be calculated if the material volume retains its circular-cylindrical shape with constant radius at a given stage of the deformation. During such a homogeneous deformation process, it is assumed

that the radius of the section decreases from the initial radius R_0 to a current radius R, while the considered length in the longitudinal direction elongates from the initial value l_0 to a current length l. The stretch ratio λ_l and longitudinal logarithmic strain ε_l along the cylinder axis can then be calculated as

$$\lambda_l = \frac{l}{l_0}, \quad \varepsilon_l = \ln\left(\lambda_l\right) \tag{1}$$

Similarly, the radial stretch ratio λ_R and the radial logarithmic strain ε_R are found as

$$\lambda_R = \frac{R}{R_0}, \quad \varepsilon_R = \ln\left(\lambda_R\right) \tag{2}$$

Assuming homogeneous deformation, λ_R and ε_R are equal in both transverse directions.

The classic volumetric stretch ratio λ_V is defined in a similar way, i.e., as the ratio between the volumes of the current and the undeformed cylinder. It can be expressed as function of λ_l and λ_R by use of Equations (1) and (2):

$$\lambda_V = \frac{V}{V_0} = \frac{\pi l R^2}{\pi l_0 {R_0}^2} = \frac{\lambda_l l_0 \left(\lambda_R R_0\right)^2}{l_0 {R_0}^2} = \lambda_l \lambda_R^2 \tag{3}$$

It is then straightforward to calculate the classic volumetric logarithmic strain ε_V as

$$\varepsilon_V = \ln\left(\lambda_V\right) = \ln\left(\lambda_l\right) + 2\ln\left(\lambda_R\right) = \varepsilon_l + 2\varepsilon_R \tag{4}$$

This well-known relation can also be applied in tension tests where the sample has a rectangular cross section if the strain ε_R (or stretch ratio λ_R) is exchanged with the appropriate deformation measures in the width and thickness direction. Again, the deformation is supposed to be homogeneous.

2.2. Parabolic method

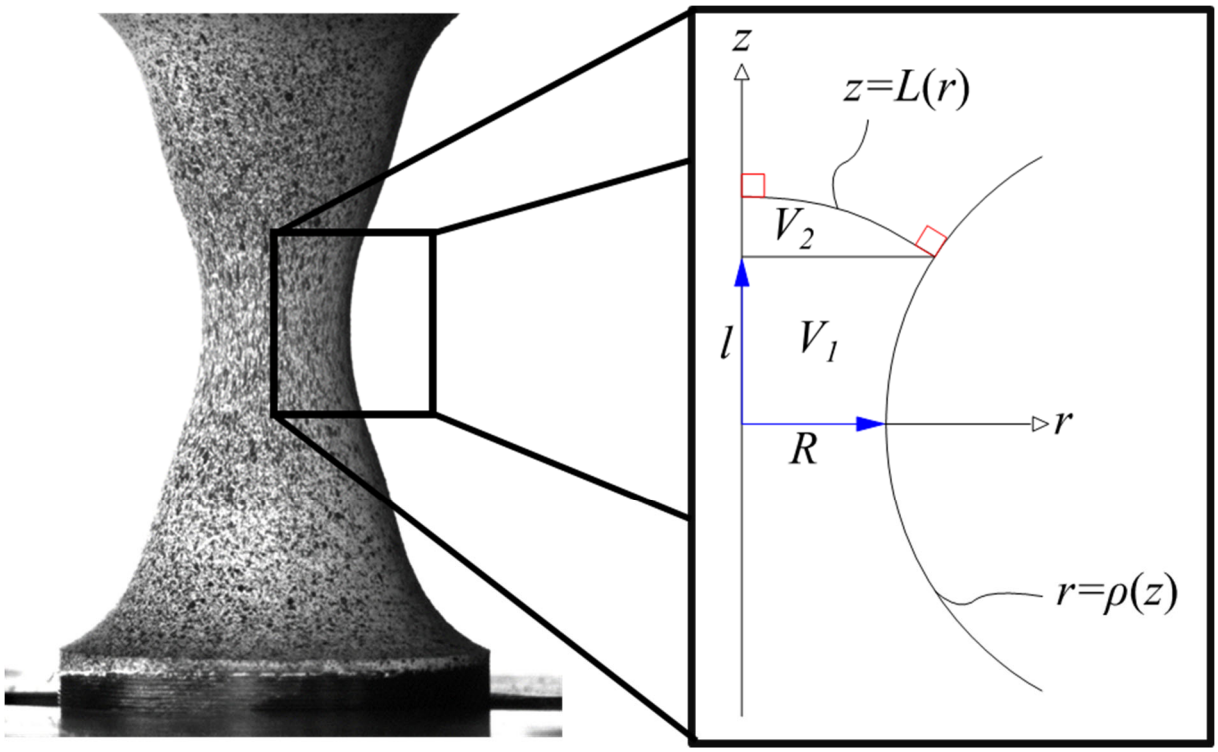

Figure 1: Sketch of the geometry in the post-necking phase of an axi-symmetric uniaxial tension test specimen. The z axis is coincident with the symmetry axis.

Calculation of the volumetric strain in a necked section requires a more careful analysis than the classic approach outlined in the previous section. Figure 1 shows the boundary and the longitudinal axis (z axis) of an axisymmetric sample with a neck. The radial axis (r axis) is located in the section at the center of the neck with current radius R, which implies that R represents the minimum radius of the sample. It is assumed that the shape of the neck's surface can be expressed by the planar curve $r = \rho(z)$ given as

$$r = \rho(z) = \frac{\kappa}{2} z^2 + R \tag{5}$$

where κ is the curvature of the neck. A key hypothesis for the deformation field in the neck is that any material element located at the surface must rotate with the surface as the neck forms. This is a consequence of the absence of shear stresses on the free surface. If we introduce a planar curve $z = L(r)$ spanning between the center of the sample and the surface, see Figure 1, we can define three constraints for this curve:

$$\left.\frac{dL}{dr}\right|_{r=0} = 0 \tag{6}$$

$$\left.\frac{dL}{dr}\right|_{r=\rho(l)} = -\left.\frac{d\rho}{dz}\right|_{z=l} \tag{7}$$

$$L\left(r=\rho\left(l\right)\right)=l \tag{8}$$

The first of these constraints states that the planar curve $z=L\left(r\right)$ inside the material is perpendicular to the longitudinal axis at the longitudinal symmetry axis $r=0$. Further, as shown in Figure 1, it is perpendicular to the surface curve $r=\rho\left(z\right)$ at the intersection point $\left(r,z\right)=\left(\rho\left(l\right),l\right)$. Assuming a second order polynomial in r for $z=L\left(r\right)$ and solving for the three constraints defined by Equations (6) to (8), we get

$$L\left(r\right) = \frac{1}{2}\rho'\left(l\right)\left(\rho\left(l\right)-\frac{r^2}{\rho\left(l\right)}\right)+l = \frac{\kappa l}{2}\left(\frac{\kappa l^2}{2}+R-\frac{r^2}{\frac{\kappa l^2}{2}+R}\right)+l \tag{9}$$

for $0\le r\le\rho\left(l\right)$, and where $\rho'\left(l\right)$ is $d\rho/dz$ evaluated at $z=l$. It is now possible to calculate the volume $V=V_1+V_2$ of the solid of revolution in Figure 1 as

$$\begin{aligned} V\left(l\right) &= \int_0^l \pi\rho\left(z\right)^2 dz + \int_0^{\rho(l)} 2\pi r\left(L\left(r\right)-l\right)dr \\ &= \pi l\left(R^2+\frac{R\kappa l^2}{3}+\frac{\kappa^2 l^4}{20}\right)+\frac{\kappa l\pi}{4}\left(R+\frac{\kappa l^2}{2}\right)^3 \end{aligned} \tag{10}$$

for a given shape of the neck as defined by the curvature κ and minimum radius R. Dividing by the initial volume of the solid of revolution $V_0=\pi l_0 R_0^2$ and inserting $l=\lambda_l l_0$, we get the volume ratio as

$$\lambda_V=\frac{V}{V_0}=\lambda_l\lambda_R^2\left[\left(1+\frac{\kappa\left(\lambda_l l_0\right)^2}{3R}+\frac{\kappa^2\left(\lambda_l l_0\right)^4}{20R^2}\right)+\frac{\kappa R}{4}\left(1+\frac{\kappa\left(\lambda_l l_0\right)^2}{2R}\right)^3\right] \tag{11}$$

If we consider the volume of a thin disc of material in the center of neck so that $l_0 \to dl_0$ and neglect higher order terms in the infinitesimal length dl_0, we get the following approximation for the volumetric stretch ratio

$$\lambda_V = \lambda_l \lambda_R^2 \left(1 + \frac{\kappa R}{4} \right) \tag{12}$$

The corresponding volumetric logarithmic strain reads

$$\varepsilon_V = \ln\left(\lambda_V\right) = \varepsilon_l + 2\varepsilon_R + \ln\left(1 + \frac{R\kappa}{4} \right) \tag{13}$$

Note that λ_R and $\varepsilon_R = \ln \lambda_R$ are now average quantities over the radius of the minimum cross-section of the specimen. It is seen that Equation (13) contains Equation (3) as a special case when the curvature κ is equal to zero, which corresponds to a sustained circular-cylindrical shape of the sample section (no necking). Based on surface measurements only, Equation (13) is hence an improved approximation for the volumetric strain of a thin slice of material situated at the center of a neck with a finite area $A = \pi R^2$ and an infinitesimal outer length $dl = \lambda_l dl_0$. The improved formula for the volumetric strain is only based on surface geometry. Hence, it does not address the mechanism behind the volumetric dilatation.

This method is hereafter referred to as the "parabolic method". It should also be noted that the same analysis applies to a pre-notched sample, where the only change would be to introduce the change in curvature relative to the initial curvature of the notch as variable κ. Concerning the choice of deformation field as defined with the planar curve $z = L\left(r\right)$, a similar set of assumptions was used on uniaxial tension tests to recreate the full strain field from surface measurements by Rossi et al. [21] in a recent paper.

2.3. Evaluation of the parabolic vs. the classic method

Since the deformation of steel and other metals normally is assumed to be isochoric, i.e., volume preserving, in the plastic domain, the performance of the parabolic method given in Equation (13) is illustrated by applying it to a uniaxial tension test of an M16 steel bolt of grade 8.8. In the test, which was reported by Grimsmo et al. [32], the bolt was fixed through its head and a nut in the testing machine, and had a slightly reduced diameter in the gauge area. A single frame of the bolt with data gathered by DIC and edge tracing is shown in Figure 2, where the bolt is depicted in its ultimate state immediately before failure. Clearly, a pronounced neck is present.

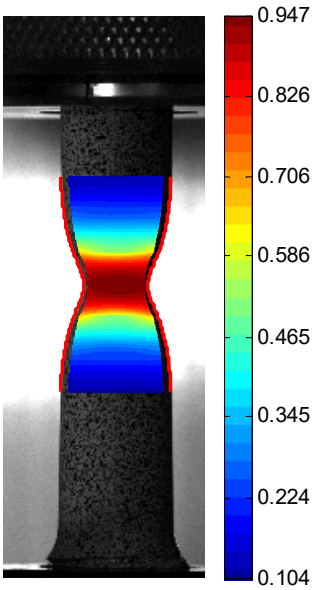

Figure 2: M16 steel bolt stretched in uniaxial tension and analyzed with DIC and edge tracing. The color bar indicates levels of longitudinal logarithmic strain.

Figure 3(a) shows the neck curvature as function of the local longitudinal strain in the minimum section of the neck. It appears that the onset of necking occurs at $\varepsilon_l \simeq 0.1$, while the local strain at failure approaches 1. Further, it can be seen that the curvature increases almost linearly with the longitudinal strain after the onset of necking.

It is now possible to compute the local volumetric strain with both the classic and the parabolic method. The resulting volumetric strains are shown in Figure 3(b). Substantial negative values after the onset of necking are observed for the classic volumetric strain calculated with Equation (4), and it evolves in a more or less linear fashion with the longitudinal strain. In contrast, Figure 3(b) shows that the resulting volumetric strain indeed is close to zero when Equation (13) is adopted instead. Thus, this benchmark test on an incompressible metallic material validates the applicability of the parabolic method, defined by Equations (12) and (13), for calculation of the volume change in a necked tensile sample. This benchmark serves as an extreme case, since κR reaches a value close to unity.

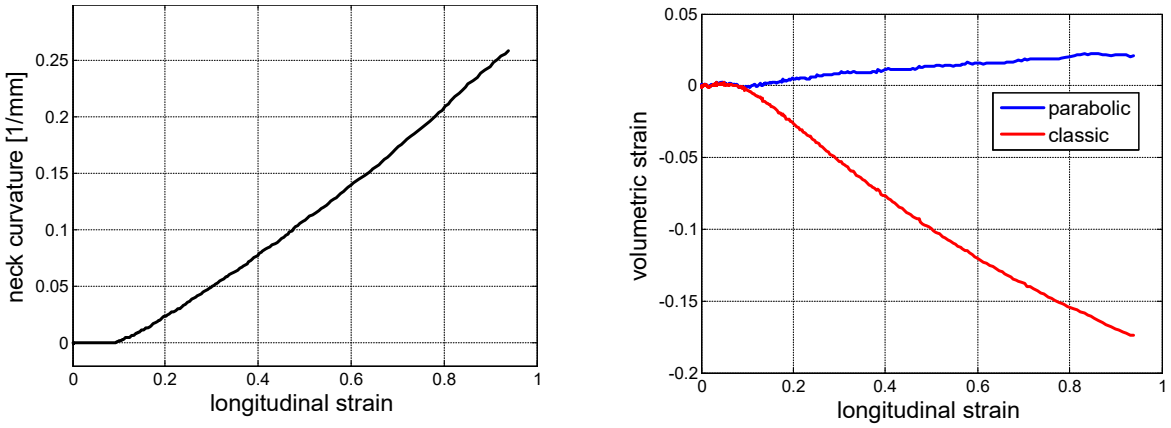

(a) (b)

Figure 3: (a) Curvature and (b) volumetric strain versus longitudinal strain at the center of the neck of a M16 steel bolt subjected to uniaxial tension. The volumetric strain is calculated using the classic and the parabolic method.

3. Volumetric strains in uniaxial tension tests on HDPE and PVC

3.1. Materials and specimens

Uniaxial tension tests of a semi-crystalline high density polyethylene (HDPE) and an amorphous poly-vinyl chloride (PVC) were employed to compare the volumetric strains calculated with Equations (4) and (13), respectively. Both materials were acquired as 10 mm thick off-the-shelf extruded plates from a wholesaler. They are hence commercial polymer blends with particle inclusions and filler material. The specifications of the blends were not provided by the manufacturer.

Figure 4 and Figure 5 show the tension test specimens. The comparatively thick plates allowed for axisymmetric samples cut on the lathe. The rather short gauge section length of 8 mm and 4 mm for HDPE and PVC, respectively, deviates from the measures recommended in the ISO standard for tension tests of polymeric materials [33]. Moreover, the transition zone between the gauge section and the clamping part of the samples has a rather small diameter of 6 mm. Our choice is motivated by the instrumentation protocol involving a digital camera and subsequent determination of the deformation with DIC, see Section 3.2. It is then favorable to have a short gauge section and small shoulder radius to allow for a sufficiently good resolution of the digital pictures taken in the last stage of the tension tests, i.e., when the stress increases significantly after the cold drawing plateau. The logarithmic strain may approach 2 in this phase of the deformation process. A comparatively long gauge section as suggested by the ISO standard [33], implies that the overall length of the sample is very large when the cold drawing process has finished, and the camera view must be adapted such that the entire gauge part in its deformed state is covered by the digital pictures. The consequence is reduced resolution and hence inferior accuracy of the strains measured with DIC.

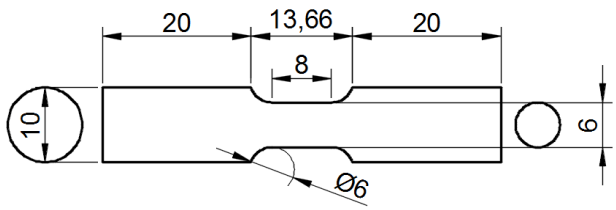

Figure 4: Geometry of uniaxial tension sample for HDPE [mm].

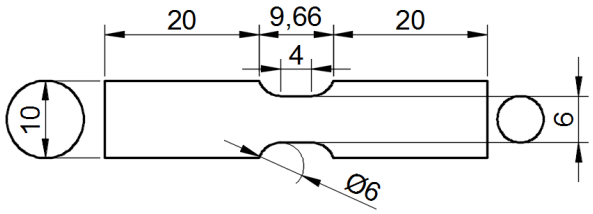

Figure 5: Geometry of uniaxial tension sample for PVC [mm].

Six samples were made for each of the two materials. They were tested at three different cross-head velocities giving constant nominal strain rates of $10^{-2.5}$, $10^{-2.0}$ and $10^{-1.5}$ s^{-1}, with two replicate tests per nominal strain rate.

3.2. Experimental set-up

The experimental setup is shown in Figure 6, where it is seen that the sample (d) is monitored by a single digital camera (a) positioned at approximately one meter distance. The 5 MP CCD camera was equipped with a zoom lens. The frame acquisition rate was adjusted with the nominal strain rate of the test in such a way that approx. 800 digital pictures were available for each test. A noteworthy aspect of the setup is the two LED lights. A sample light (b) is used to illuminate the sample, while a background light (c) illuminates a sheet of aluminum (e) that is placed directly behind the sample, relative to the observing camera (a). The aluminum sheet serves to scatter the light, creating a burned-out white background in the digital pictures. This ensures a significant contrast of the grayscale value in the digital pictures between the sample and the background, which in turn is beneficial for the subsequent edge tracing in the post processing of the image data.

The element based DIC algorithm described by Andersen [22] is used to obtain local values of the longitudinal stretch ratio λ_l and thus the longitudinal logarithmic strain ε_l. The DIC algorithm employs higher order displacement elements with 16 nodes, facilitating an improvement of the representation of the strain field at and close to the neck. An initial element size of 80×80 pixels is used with a bicubic pixel interpolation. To measure the curvature κ of the neck and the minimum radius R of the necked section, an edge tracing algorithm was employed [22]. The algorithm uses a simple grayscale gradient search combined with a method for defining the longitudinal center axis of sample.

All tests were instrumented with one single camera, which possibly can create some artefacts in the measurements. The problem arises when a material surface moves away from or towards the camera. Such an out-of-plane rigid body motion is captured as an in-plane deformation in the DIC analysis. This artificial deformation is proportional to the relation $1+\Delta x / X$ where Δx is the distance a surface has moved away from the camera and X is the initial distance from the camera. For these tests, a zoom lens was used, with the camera placed approximately one meter from the samples. This results in a negligible artificial strain, and would at worst result in downscaling any line segment length by a factor of 0.997 with the setup and sample radius used here [22]. It is reasonable to assume that image points on the edges of the sample do not change distance to the camera. Radial measurements from edge tracing are hence unaffected.

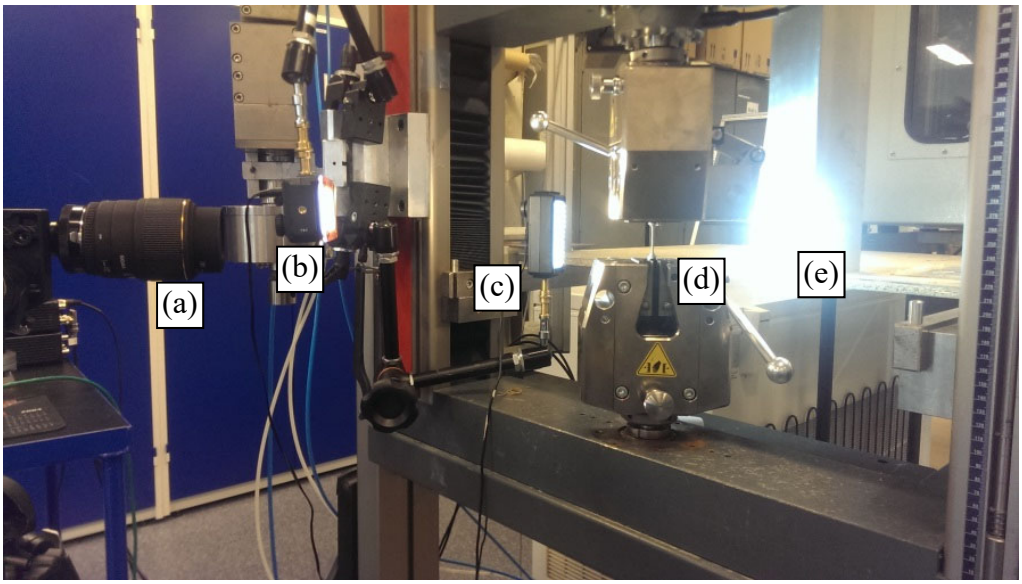

Figure 6: Test setup involving (a) camera with macro lens, (b) sample lighting, (c) background lighting, (d) sample, and (e) aluminum sheet giving a diffuse reflective background.

3.3. Experimental results

Addressing a nominal strain rate of $10^{-2.5}$ s^{-1}, images of a sample before and during deformation are shown for both materials in Figure 7. The deformed images were taken when the applied force had reached an almost constant value, corresponding to cold-drawing deformation. Clearly, there is a significantly more pronounced localization in HDPE than in PVC.

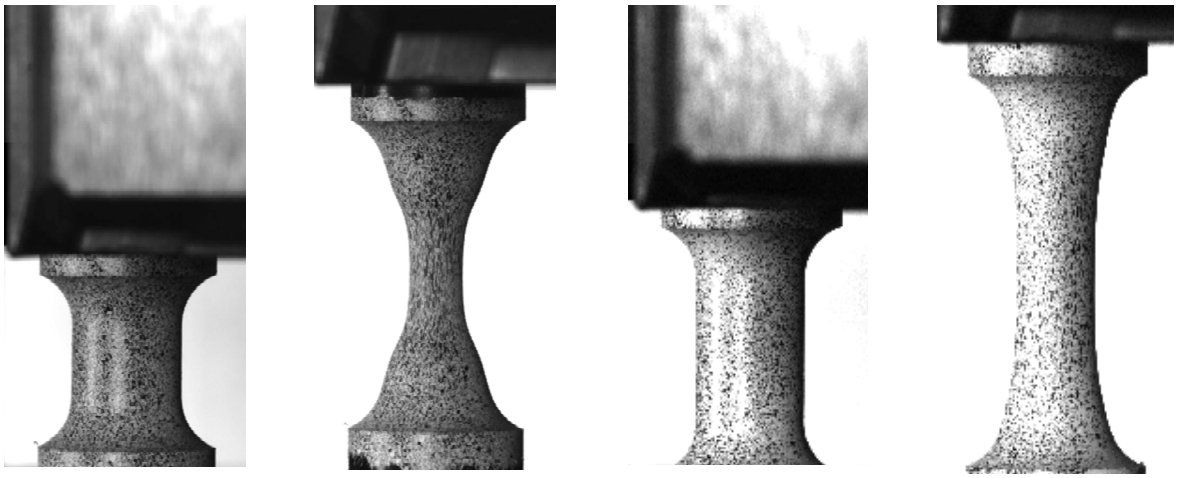

(a) (b)

Figure 7: Undeformed and deformed configurations of (a) HDPE and (b) PVC samples, where the deformed configuration refers to a stage after initiation of cold drawing. Both samples were stretched at a nominal strain rate of $10^{-2.5}$ s^{-1}

The minimum radius R of the necked section as a function of longitudinal logarithmic strain ε_l is shown in Figure 8 for both materials. The radius is found by tracing the edge of the samples, and the longitudinal strain is measured locally using DIC. The radius decreases monotonically from the initial value of 3 mm. It is noted that there is a change of slope at a certain strain level for both materials. For HDPE the slope is reduced at $\varepsilon_l \approx 0.5$, while for PVC the slope increases when $\varepsilon_l \approx 0.2$. This can indicate a change in the volumetric strain rate, but since curvature is yet to be considered, one variable in Equation (13) is still missing. Another observation is that the reduction of radius seems to be independent of the strain rate.

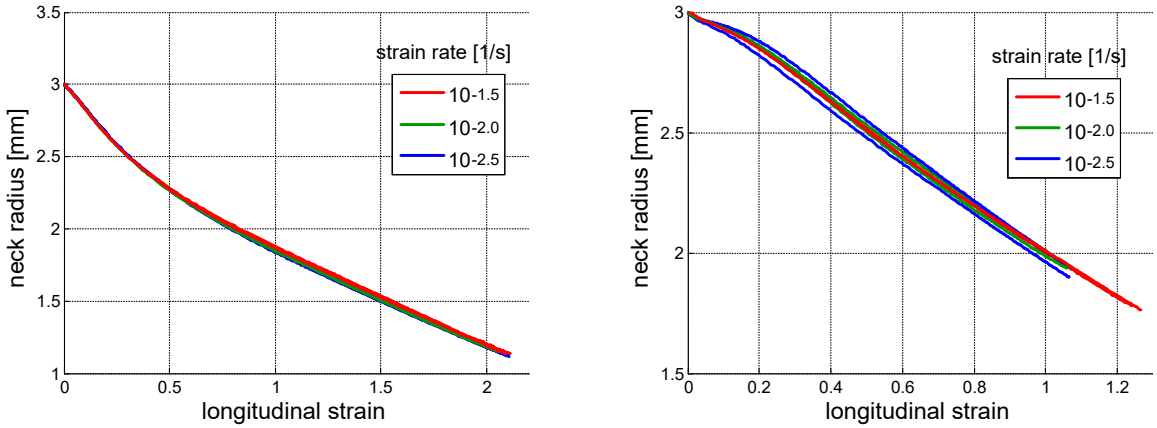

(a) (b)

Figure 8: Neck radius versus longitudinal logarithmic strain for (a) HDPE and (b) PVC.

The curvature of the neck κ as function of longitudinal logarithmic strain ε_l is shown for both materials and all samples in Figure 9. A significant difference can be seen between the two materials. The neck curvature of the HDPE samples increases until a maximum curvature of approx. 0.2 mm^{-1} is reached when $\varepsilon_l \simeq 0.8$. Thereafter, the curvature decreases gradually towards zero with increasing strain. A curvature approaching zero corresponds to cold drawing of the necked section, where the neck eventually disappears. It is observed that the curvature of the HDPE samples experiences only a minor influence of strain rate. For PVC, on the other hand, a trend of higher curvatures at higher strain rates is present, but the measured curvature is much smaller than for HDPE. The curvature is gradually reduced when the longitudinal strain exceeds $\varepsilon_l \simeq 0.6$. The large difference in curvature between the two materials quantifies the visual difference of the localization zones observed in Figure 7. A possible explanation for the comparatively larger strain-rate sensitivity seen for PVC is that this material seems to experience substantial thermal softening as a consequence of self-heating [22].

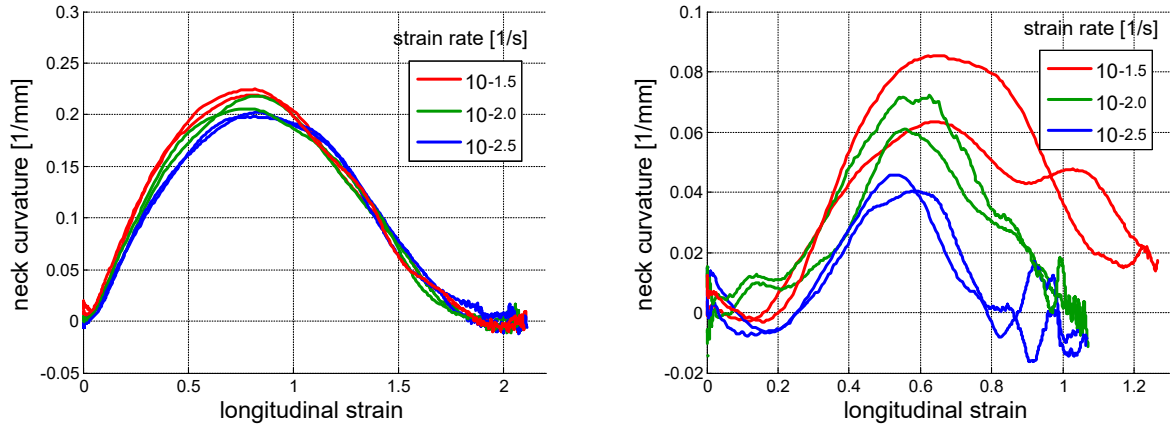

(a) (b)

Figure 9: Neck curvature versus longitudinal logarithmic strain for (a) HDPE and (b) PVC.

With radial and longitudinal strains and curvature measured, it is now possible to calculate the volumetric strain applying both the classic method and the parabolic method.

Figure 10(a) and (b), respectively, show the volumetric strain calculated with the classic method, i.e. Equation (4), and the parabolic method, i.e. Equation (13), for the six tests on the HDPE material. A striking feature to notice for the classic method is the significant decrease of volume in the initial phase of the test up to a longitudinal strain of about 0.4. Moreover, an apparent strain-rate sensitivity can be seen as well as a saturation of volumetric strain at large deformations. The negative volumetric strain predicted by the classic method is not present in Figure 10(b). Now, an initial stage with negligible volumetric strain up to a longitudinal strain of 0.2 is seen, followed by an almost linear increase in volumetric strain which saturates after $\varepsilon_l \simeq 1.3$. This plateau of the volumetric-longitudinal strain curve is seen to occur much earlier than in Figure 10(a). The final level of volumetric strain, however, does not differ much between the two calculation methods.

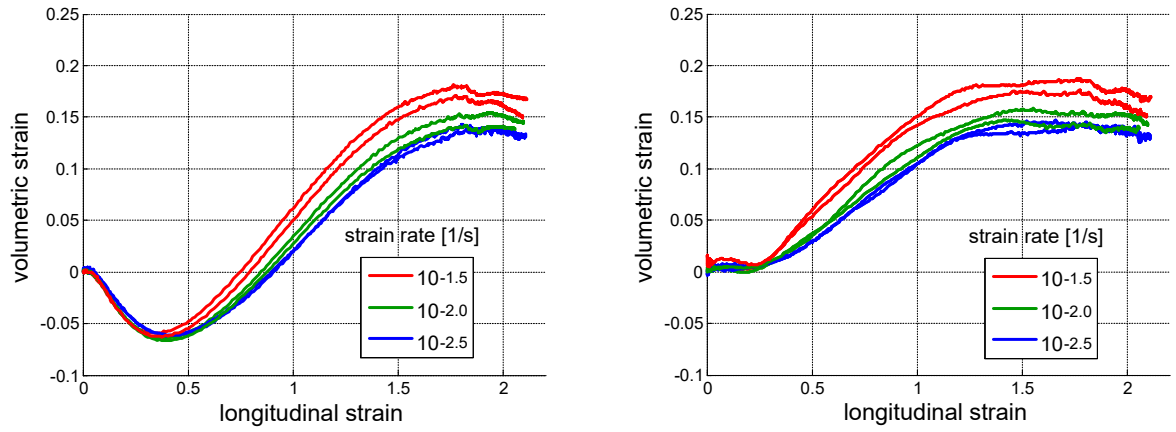

Figure 10: Volumetric versus longitudinal logarithmic strain for HDPE calculated using (a) the classic method and (b) the parabolic method.

Figure 11 shows the volumetric strain determined for the six PVC specimens. According to Figure 11(a), no negative volumetric strain is predicted with the classic method, but the slope of the volumetric-longitudinal strain curves is seen to change abruptly at a longitudinal strain around 0.2. This coincides with the stage where the curvature starts to increase, see Figure 9(b). Turning the attention to Figure 11(b), the volumetric strain saturates rather than change to the less steep slope that was predicted with the classic method. Apart from this, the difference between the volumetric strains calculated with Equations (4) and (13) is far less substantial for PVC than for HDPE. This is related to the comparatively small curvature of the neck in the PVC sample, see Figure 9, which in turn implies that the deformed shape of the PVC sample is closer to the circular-cylindrical deformation mode assumed in Equation (4).

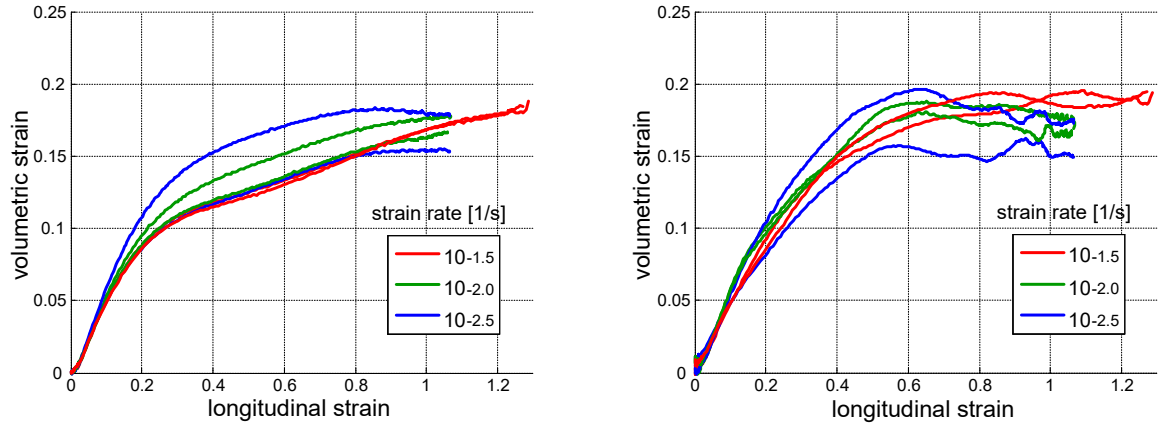

Figure 11: Volumetric versus longitudinal logarithmic strain for PVC calculated using (a) the classic method and (b) the parabolic method.

It was emphasized in Section 3.1 that the tests were carried out at three different cross-head velocities corresponding to nominal strain rates of $10^{-2.5}$, $10^{-2.0}$ and $10^{-1.5}$ s^{-1}. The use of constant

cross-head velocity results in a non-constant local strain rate when a neck forms in a specimen. Nevertheless, the tests were monitored with digital cameras, see Section 3.2, thus, the true local strain rate was measured continuously. The maximum local strain rate was found to be about 1.5 times the nominal strain rate. According to Figure 10 and Figure 11, the general trend is a slight increase in volumetric strain with increasing nominal strain rate. Yet, the three levels of nominal strain rate differ with a factor that is far larger than 1.5, and there is no indication that the deformation mechanisms change in the considered range of strain rates. Thus, there is no reason to expect that the modest increase of the local strain rate has any major influence on the shape of the neck and hence the volumetric strain during the deformation process.

3.4. Evaluation of growth mechanisms by SEM

The mechanisms behind the measured dilatation are investigated through SEM imaging performed on undeformed and stretched material samples. SEM samples were made by cooling a small piece of tested material in liquid nitrogen and then splitting it with a razor blade and a hammer. This produced a brittle fracture surface showing the interior of the samples. This technique has been described by Ognedal et al. [10]. The samples were vapor coated with gold in order to make the surface electrically conductive. The resulting micrographs are shown in Figure 12 for PVC and in Figure 13 for HDPE. As can be seen in Figure 12, PVC clearly develops cavities around filler particles during the deformation process. This is similar to what was observed by Ognedal et al. [10] in a mineral filled PVC.

The cause of dilatation in HDPE is more elusive, as can be seen from Figure 13. The material seems to have an initial porous structure which morphs into a fibrous structure with stretching. The large elongation does however make it difficult to recognize any voids. The levels of volumetric strain in Figure 10b are, however, in line with what was reported on XLPE by Johnsen et al. [18]. Moreover, Ognedal et al. [34] studied notched tension test samples made of a similar HDPE, and they showed that an increase in the stress triaxiality ratio leads to a large increase of the porosity at a given strain.

The parabolic method for calculation of the volumetric strain, see Equation (13), does only require information about the surface geometry of the sample. As such, the method is independent of the intrinsic deformation mechanisms, let it be cavitation, crazing or debonding between matrix and filler particles. In this regard, the micrographs shown in Figure 12 and Figure 13 are interesting. While there are significant voiding around particles at the microscale for PVC, another mechanism seems to be present for HDPE. However, the volumetric strain is between 0.15 and 0.20 in both cases. Varying volumetric strain in the radial direction of notched round bars has previously been reported in experimental work [3, 35], and is linked to the distribution of stresses. These papers show a distribution of volumetric strain that is qualitatively similar to the assumed field for the parabolic method proposed herein.

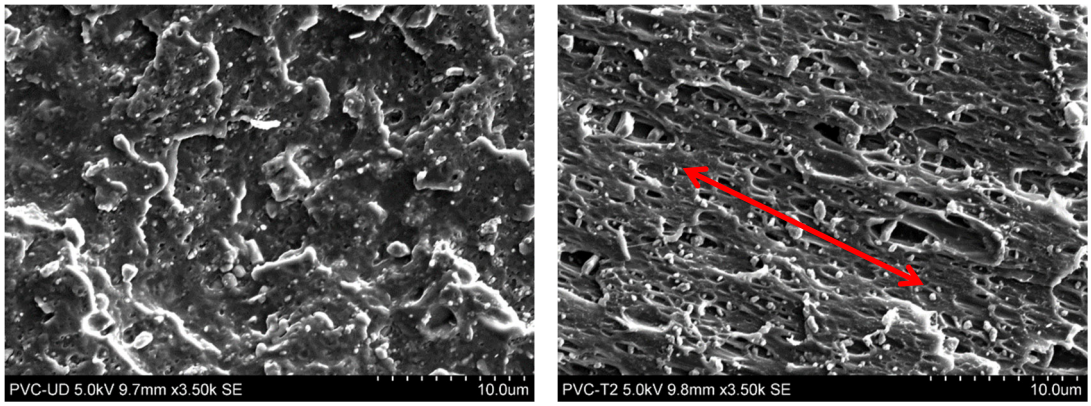

Figure 12: SEM micrographs of undeformed and deformed PVC, magnified 3500 times. The red arrow indicates the tension direction

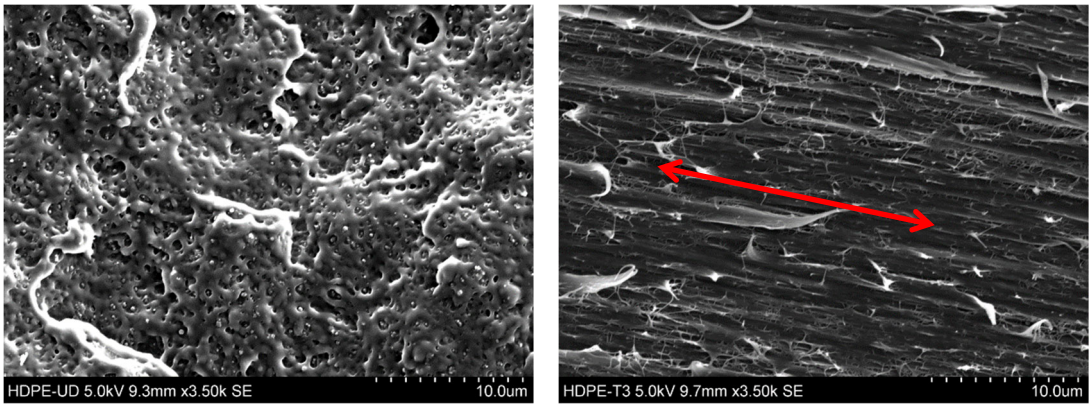

Figure 13: SEM micrographs of undeformed and deformed HDPE, magnified 3500 times. The red arrow indicates the tension direction.

4. Concluding remarks

The parabolic method for calculating volumetric strain requires information about the local longitudinal strain in the neck as well as the contour of the neck. These surface data are gathered by monitoring the test specimen with a digital camera during the deformation process. When applied to the benchmark case with a bolt made of an incompressible steel material, the parabolic method shows a significant improvement compared to the classic method. The initial negative volumetric strain observed for a HDPE material when using the classic method is completely removed when the parabolic method is employed. The difference between the classic and parabolic methods is less for the PVC material studied herein, due to less distinct necking. Yet, the saturation of the volumetric strain is not captured by the classic method. SEM micrographs indicate that the macroscopic increase of volume is accompanied by formation of voids in the material, at least for PVC. It is concluded that the parabolic method represents a significant improvement of the classic closed-form formula for calculation of volumetric strain, and that it might be relevant to have a new look at earlier results suggesting that polymers can exhibit negative volumetric strain in uniaxial tension.

Acknowledgements

The authors gratefully appreciate the financial support from the Research Council of Norway through the Centre for Advanced Structural Analysis, Project No. 237885 (SFI-CASA). The assistance from Mr Trond Auestad during the experimental test campaign is also acknowledged.

References

1. Parsons E.M., Boyce M.C., Parks D.M. and Weinberg M. (2005) Three-dimensional large-strain tensile deformation of neat and calcium carbonate-filled high-density polyethylene. *Polymer* **46**: 2257-2265.
2. Mohanraj J., Barton D.C., Ward I.M., Dahoun A., Hiver J.M. and G'Sell C. (2006) Plastic deformation and damage of polyoxymethylene in the large strain range at elevated temperatures. *Polymer* **47**: 5852-5861.
3. Boisot G., Laiarinandrasana L., Besson J., Fond C. and Hochstetter G. (2011) Experimental investigations and modeling of volume change induced by void growth in polyamide 11. *International Journal of Solids and Structures* **48**: 2642-2654.
4. Delhaye V., Clausen A.H., Moussy F., Hopperstad O.S. and Othman R. (2010) Mechanical response and microstructure investigation of a mineral and rubber modified polypropylene. *Polymer Testing* **29**: 793-802.
5. Jerabek M., Major Z., Renner K., Móczó J., Pukánszky B. and Lang R.W. (2010) Filler/matrix-debonding and micro-mechanisms of deformation in particulate filled polypropylene composites under tension. *Polymer* **51**: 2040-2048.
6. Zaïri F., Naït-Abdelaziz M., Gloaguen J.M. and Lefebvre J.M. (2011) A physically-based constitutive model for anisotropic damage in rubber-toughened glassy polymers during finite deformation. *International Journal of Plasticity* **27**: 25-51.
7. Balieu R., Lauro F., Bennani B., Delille R., Matsumoto T. and Mottola E. (2013) A fully coupled elastoviscoplastic damage model at finite strains for mineral filled semi-crystalline polymer. *International Journal of Plasticity* **51**: 241-270.
8. Johnsen J., Grytten F., Hopperstad O.S. and Clausen A.H. (2017) Influence of strain rate and temperature on the mechanical behaviour of rubber-modified polypropylene and cross-linked polyethylene. *Mechanics of Materials* **114**: 40-56.
9. Poulet P.-A., Hochstetter G., King A., Proudhon H., Joannès S. and Laiarinandrasana L. (2016) Observations by in-situ X-ray synchrotron computed tomography of the microstructural evolution of semi-crystalline Polyamide 11 during deformation. *Polymer Testing* **56**: 245-260.
10. Ognedal A.S., Clausen A.H., Berstad T., Seelig T. and Hopperstad O.S. (2014) Void nucleation and growth in mineral-filled PVC – An experimental and numerical study. *International Journal of Solids and Structures* **51**: 1494-1506.
11. Delhaye V. (2011) Behaviour and modelling of polymers for crash applications. PhD, NTNU.
12. Ward I.M. and Sweeney J. (2012) Breaking Phenomena. In: Mechanical Properties of Solid Polymers. John Wiley & Sons, Ltd: 379-447.
13. McCrum N.G., Buckley C. and Bucknall C.B. (1997) *Principles of polymer engineering* Oxford University Press, USA.
14. Halary J.L., Lauprêtre F. and Monnerie L. (2011) *Polymer materials: macroscopic properties and molecular interpretations* John Wiley & Sons.
15. G'Sell C., Hiver J.M., Dahoun A. and Souahi A. (1992) Vide-controlled tensile testing of polymers and metals beyond the necking point. *J Mater Sci* **27**: 5031-5039.
16. Rastogi P.K. (2000) *Photomechanics*. 1 edn. Springer.

17. Şerban D.A., Weber G., Marşavina L., Silberschmidt V.V. and Hufenbach W. (2013) Tensile properties of semi-crystalline thermoplastic polymers: Effects of temperature and strain rates. *Polymer Testing* **32**: 413-425.
18. Johnsen J., Grytten F., Hopperstad O.S. and Clausen A.H. (2016) Experimental set-up for determination of the large-strain tensile behaviour of polymers at low temperatures. *Polymer Testing* **53**: 305-313.
19. Grytten F., Daiyan H., Polanco-Loria M. and Dumoulin S. (2009) Use of digital image correlation to measure large-strain tensile properties of ductile thermoplastics. *Polymer Testing* **28**: 653-660.
20. Delhaye V., Clausen A.H., Moussy F., Othman R. and Hopperstad O.S. (2011) Influence of stress state and strain rate on the behaviour of a rubber-particle reinforced polypropylene. *International Journal of Impact Engineering* **38**: 208-218.
21. Rossi M., Cortese L., Genovese K., Lattanzi A., Nalli F. and Pierron F. (2018) Evaluation of Volume Deformation from Surface DIC Measurement. *Exp Mech* **58**: 1181-1194.
22. Andersen M. (2016) An Experimental and Numerical Study of Thermoplastics at Large Deformations. Phd, NTNU.
23. Vilamosa V., Clausen A.H., Fagerholt E., Hopperstad O.S. and Børvik T. (2014) Local Measurement of Stress–Strain Behaviour of Ductile Materials at Elevated Temperatures in a Split-Hopkinson Tension Bar System. *Strain* **50**: 223-235.
24. Addiego F., Dahoun A., G'Sell C. and Hiver J.-M. (2006) Characterization of volume strain at large deformation under uniaxial tension in high-density polyethylene. *Polymer* **47**: 4387-4399.
25. G'Sell C., Hiver J.M. and Dahoun A. (2002) Experimental characterization of deformation damage in solid polymers under tension, and its interrelation with necking. *International Journal of Solids and Structures* **39**: 3857-3872.
26. Dahoun A., Aboulfaraj M., G'Sell C., Molinari A. and Canova G.R. (1995) Plastic behavior and deformation textures of poly(etherether ketone) under uniaxial tension and simple shear. *Polymer Engineering & Science* **35**: 317-330.
27. Powers J.M. and Caddell R.M. (1972) The macroscopic volume changes of selected polymers subjected to uniform tensile deformation. *Polymer Engineering & Science* **12**: 432-436.
28. Tang H.I., Hiltner A. and Baer E. (1987) Biaxial orientation of polypropylene by hydrostatic solid state extrusion. Part III: Mechanical properties and deformation mechanisms. *Polymer Engineering & Science* **27**: 876-886.
29. Gaucher–Miri V., Depecker C. and Séguéla R. (1997) Reversible strain-induced order in the amorphous phase of a low-density ethylene/butene copolymer. *Journal of Polymer Science Part B: Polymer Physics* **35**: 2151-2159.
30. Laiarinandrasana L., Klinkova O., Nguyen F., Proudhon H., Morgeneyer T.F. and Ludwig W. (2016) Three dimensional quantification of anisotropic void evolution in deformed semi-crystalline polyamide 6. *International Journal of Plasticity* **83**: 19-36.
31. Brusselle-Dupend N., Rosenberg E. and Adrien J. (2011) Characterization of cavitation development while tensile testing PVF2 using 3D X-ray microtomography. *Materials Science and Engineering: A* **530**: 36-50.
32. Grimsmo E.L., Clausen A.H., Aalberg A. and Langseth M. (2016) A numerical study of beam-to-column joints subjected to impact. *Engineering Structures* **120**: 103-115.
33. Standard N. (2012) ISO 527-2:2012. In: Book ISO 527-2:2012, Editor (Ed)^(Eds). Standard Norge, City.
34. Ognedal A.S., Clausen A.H., Dahlen A. and Hopperstad O.S. (2014) Behavior of PVC and HDPE under highly triaxial stress states: An experimental and numerical study. *Mechanics of Materials* **72**: 94-108.
35. Selles N., Saintier N. and Laiarinandrasana L. (2016) Voiding mechanisms in semi-crystalline polyamide 6 during creep tests assessed by damage based constitutive relationships and finite elements calculations. *International Journal of Plasticity* **86**: 112-127.